
Molecular Simulation of Gas Solubility in Nitrile Butadiene Rubber

M. Khawaja[†], A.P. Sutton[†] and A.A. Mostofi^{†‡}

[†] *Department of Physics and the Thomas Young Centre for Theory and Simulation of Materials, Imperial College London, London SW7 2AZ, UK*

[‡] *Department of Materials and the Thomas Young Centre for Theory and Simulation of Materials, Imperial College London SW7 2AZ, UK*

1 Inhomogeneity of insertions

To illustrate the inhomogeneity of ‘successful’ insertions in the polymer, i.e., those that contribute to the solubility, insertions were performed using unbiased Widom insertion and the resulting positions and accompanying Boltzmann factors were binned along one side of the cubic simulation cell, which was chosen to be along the y -direction, without loss of generality. We define the fractional co-ordinate in the y direction, $y' = y/L_y$, where L_y is the length of the supercell, and y' is in the range $[0, 1)$. The solubility in a bin of width w centred at y' is

$$s(y') = \frac{\sum_{i=1}^N \exp(-\Delta E_i/k_B T) g(L_y(Y'_i - y')/w)}{\sum_{i=1}^N g(L_y(Y'_i - y')/w)}, \quad (1)$$

where insertion i is at fractional co-ordinate Y'_i , with corresponding insertion energy ΔE_i , N insertions are performed in total and $g(x)$ is a top hat function given by

$$g(x) = \begin{cases} 0 & |x| \geq \frac{1}{2} \\ 1 & |x| < \frac{1}{2} \end{cases}. \quad (2)$$

The effect of varying the number of snapshots, m , taken from a long molecular dynamics run from each of n independent initial configurations can then be investigated by averaging $s(y')$ over different combinations of $n \times m$. Only the subset of insertions whose insertion energies were less than $5k_B T$ ($T = 25^\circ\text{C}$) were written and sorted, as they represent the small minority of insertions which contribute a non-negligible amount to the solubility. This requires changing the normalisation factor in Eqn. (1) from the actual number of insertions per bin to the expected number of insertions per bin:

$$s(y') = \frac{\sum_{i=1}^N \exp(-\Delta E_i/k_B T) g(L_y(Y'_i - y')/w)}{Nw/L_y}. \quad (3)$$

The results are shown in Figure S1a.

The standard deviation in this solubility distribution is calculated as a percentage of the average solubility, as a function of n and m , and is shown in Figure S1b. Figures S1a and S1b show that the distribution becomes more homogeneous when n and m are increased. The bin size was 5% of the length of the supercell, 0.23 nm wide on average.

Whilst Figure S1a shows that even with 24 independent configurations, and 250 snapshots for each of them, the solubility distribution is not entirely homogeneous, Figure S1b shows that increasing n , m , beyond these values yields diminishing returns.

Figure S2 shows regions within a single snapshot of an equilibrated supercell of NBR where the solubilities of CO_2 , H_2O and helium are relatively high. Insertions are performed using the unbiased Widom insertion technique, and the associated Boltzmann factors are sorted into a 3D grid of $100 \times 100 \times 100$ voxels based on the position of the centre-of-mass of the inserted molecule. Summing over the Boltzmann factors within a voxel and dividing by the total number of insertions performed gives the local solubility. Regions where the local solubility is less than 10^{-8} are not shown. As CO_2 is the largest molecule of the three there are relatively few regions where its solubility is significant, whereas helium is more homogeneously distributed. Water is more homogeneously distributed in the snapshot and its local solubilities are greater than those of CO_2 . We speculate that the former is due to the smaller van der Waals volume of water and the latter is due to the electrostatic interaction between its dipole and dipoles in the elastomer, such as the $\text{C}\equiv\text{N}$ bond in ACN, which is a stronger and longer-ranged interaction than CO_2 can achieve through its quadrupole. For all three molecular species successful insertions are very localised, indicating that the biased Widom insertion technique would be more efficient.

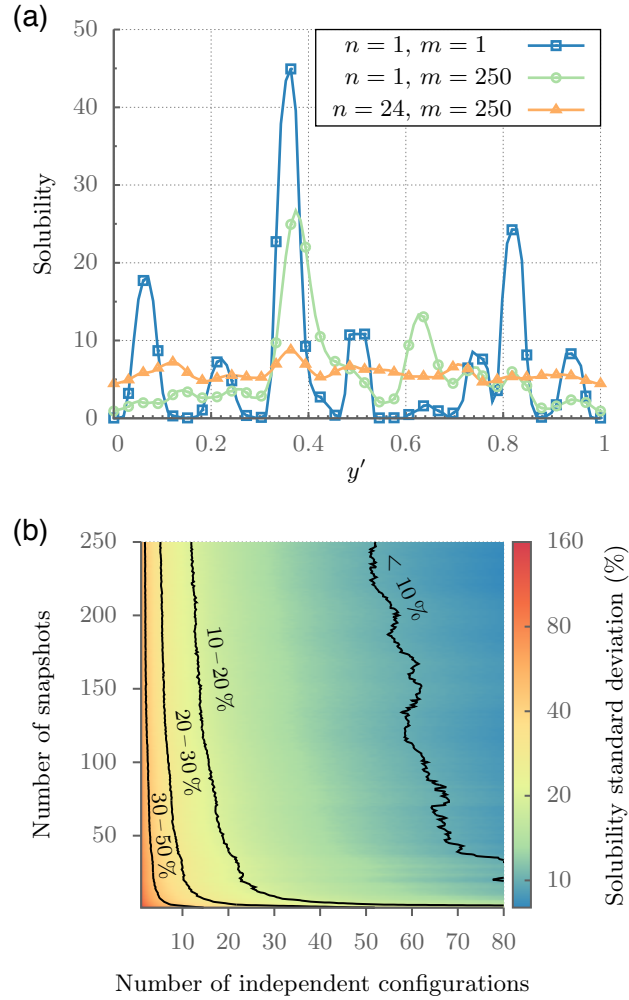


Figure S1: (a) Distributions of computed solubility of CO₂ as a function of the normalised position y' along one side of the supercell, plotted for different numbers of independently generated configurations (n) and dynamically evolved snapshots (m). (b) Percentage standard deviation in the solubility distributions from their average values, as a function of n and m , where randomised resampling has been used to smooth the fluctuations that would otherwise dominate for small n . Insertions performed using the unbiased Widom insertion technique with $N = 10^8$.

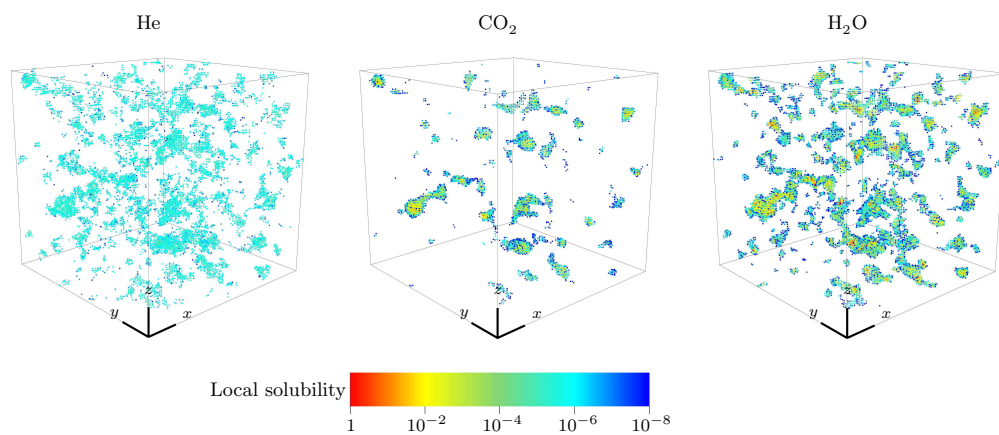


Figure S2: Local solubilities of CO₂, H₂O and helium in the same snapshot of NBR. Only cells with local solubility higher than 10⁻⁸ are shown. Insertions performed using unbiased Widom insertion technique with $N = 10^8$. Image generated using VisIt.[1]

2 Effect of free volume on the convergence of the biased Widom insertion technique

Figure S3 shows the solubility of CO₂ error as a function of the number of grid points per dimension, $N_{\text{grid}}^{\frac{1}{3}}$. The number of insertions per voxel centred on each grid point of width $L/N_{\text{grid}}^{\frac{1}{3}}$ for a cubic simulation cell of length L , is fixed at 100, and $\alpha = 0.2$. The error-bars represent the standard error, and are approximately 3% of the solubility. From this data it is inferred that 100 grid points per dimension is sufficient to achieve reasonable convergence.

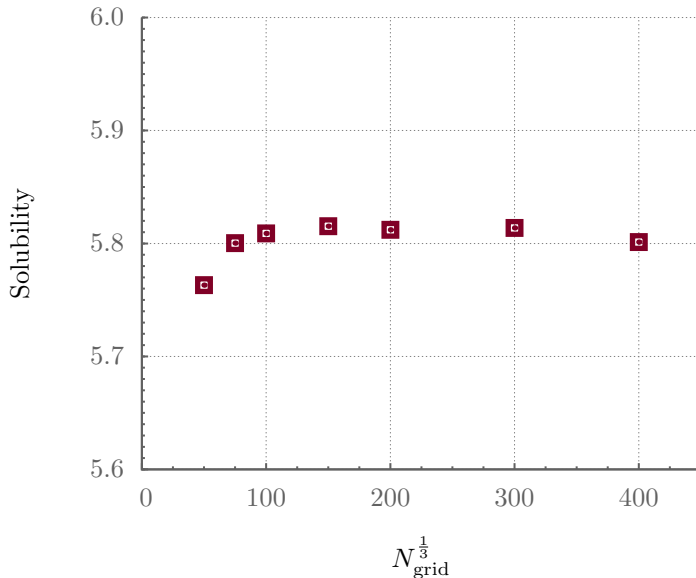


Figure S3: Convergence of CO₂ solubility with number of grid points per dimension, $N_{\text{grid}}^{\frac{1}{3}}$. NBR of 41.3% ACN content generated at STP, 100 insertions per grid point, $\alpha = 0.2$.

Figure S4 shows the effect of the free-volume tuning parameter, α , on the solubility of CO₂ as well as the fractional free-volume (FFV). For large, negative values of α , the lack of free-volume sites in which to perform insertions means that the solubility is far from its converged value. For values above approximately 0.15, the solubility becomes independent of α , and, since the computational cost of particle insertion scales approximately linearly with the number of insertions, which in this case is proportional to the FFV, a conservative value of $\alpha = 0.2$ is chosen, corresponding to an average FFV and standard deviation of $(2.55 \pm 0.07)\%$, i.e., approximately 40 times faster than the random insertions for the same number of insertions per unit volume.

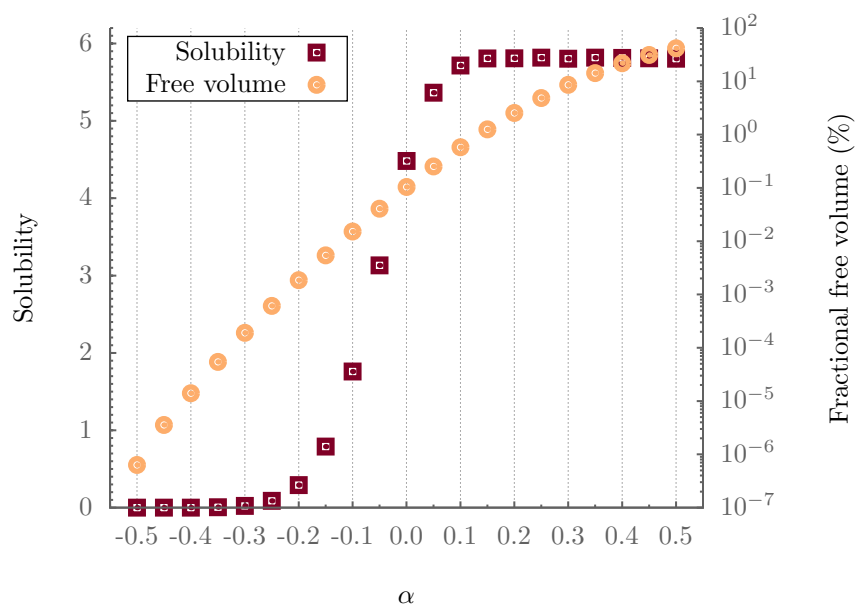


Figure S4: Convergence of CO_2 solubility and polymer free-volume with α , a parameter used to tune the radius, $r = (1 - \alpha)\sqrt{\sigma_{\text{He}}\sigma_j}$, used to define the free volume, where σ_{He} and σ_j are the Lennard-Jones radii of helium (0.2556 nm) and atom j of the polymer, in the OPLS-AA force-field. NBR of 41.3% ACN content generated at STP, 100 insertions per grid point, 10^6 grid points.

References

- [1] Hank Childs, Eric Brugger, Brad Whitlock, Jeremy Meredith, Sean Ahern, David Pugmire, Kathleen Biagas, Mark Miller, Cyrus Harrison, Gunther H. Weber, et al. VisIt: An End-User Tool For Visualizing and Analyzing Very Large Data. In *High Performance Visualization—Enabling Extreme-Scale Scientific Insight*, pages 357–372. Oct 2012.